A Multichannel Surface EMG System for Hand Motion Recognition

Article *in* International Journal of Humanoid Robotics · March 2015

DOI: 10.1142/S0219843615500115

CITATIONS
82

READS
1,106

4 authors:

Yinfeng Fang
Hangzhou Dianzi University
43 PUBLICATIONS **551** CITATIONS
SEE PROFILE

Honghai Liu
University of Portsmouth
306 PUBLICATIONS **4,598** CITATIONS
SEE PROFILE

Gongfa Li
Wuhan University of Science and Technology
269 PUBLICATIONS **1,230** CITATIONS
SEE PROFILE

Xiangyang Zhu
Shanghai Jiao Tong University
195 PUBLICATIONS **2,332** CITATIONS
SEE PROFILE

International Journal of Humanoid Robotics
Vol. 12, No. 2 (2015) 1550011 (13 pages)

DOI: 10.1142/S0219843615500115

World Scientific
www.worldscientific.com

A Multichannel Surface EMG System for Hand Motion Recognition

Yinfeng Fang[*,‡] and Honghai Liu[†,*,§]

[*]*Intelligent Systems and Biomedical Robotics Group, School of Computing, University of Portsmouth, Portsmouth, PO1 3HE, United Kingdom*

[†]*State Key Laboratory of Mechanical System and Vibration, Shanghai Jiao Tong University, Shanghai 200240, P. R. China*
[‡]*yinfeng.fang@port.ac.uk*
[§]*honghai.liu@port.ac.uk*

Gongfa Li

College of Machinery and Automation, Wuhan University of Science and Technology, Wuhan 430081, P. R. China
ligongfa@wust.edu.cn

Xiangyang Zhu

State Key Laboratory of Mechanical System and Vibration, Shanghai Jiao Tong University, Shanghai 200240, P. R. China
mexyzhu@sjtu.edu.cn

Received 19 May 2014
Accepted 8 February 2015
Published 30 March 2015

Surface electromyography (sEMG)-based hand motion recognition has a variety of promising applications. While a person performs different hand motions, commands can be extracted to control external devices, such as prosthetic hands, tablets and so forth. The acquisition of discriminative sEMG signals determines the accuracy of intended control commands extraction. This paper develops an 16-channel sEMG signal acquisition system with a novel electrode configuration that is specially designed to collect sEMG on the forearm. Besides, to establish the relationship between multichannel sEMG signals and hand motions, a 2D EMG map is designed. Inspired from the electromyographic (EMG) map, this paper proposes an EMG feature named differential root mean square (DRMS) that somewhat takes the relationship between neighboring EMG channels into account. In the task of four hand motion discrimination by K-means and fuzzy C-means, DRMS

[§]Corresponding author.

outperforms traditional root mean square (RMS) by 29.0% and 36.8%, respectively. The findings of this paper support and guide the use of sEMG techniques to investigate sEMG-based hand motion recognition.

Keywords: Multichannel sEMG; hand motion recognition; feature; differential root mean square; EMG electrode configuration.

1. Introduction

The electromyographic (EMG) signal is the summation of the action potentials discharged by the active muscle fibers in the proximity of the recording electrodes.[1] Systematic recruitment of different forearm muscles generates various hand motions, which underlies the basic premise of this study.

Advances in the techniques of surface electro-myographic (sEMG)-based hand motion recognition contribute to its applications in diverse areas. Conventionally, data gloves and computer vision are employed to recognize hand gestures. Recently, using EMG signals to implement human machine interaction has attracted increasing attentions, since EMG is able to sense and decode human muscular activity directly and is capable of distinguishing subtle finger configurations, hand shapes and wrist movements.[2] Studies regarding hand motion based human machine interface can be found in Ref. 2–10.

Although significant efforts have been made to EMG-based hand motion recognition, it is still a challenge to be implemented in practice. This paper concentrates on several factors as follows. First of all, sEMG electrode configuration is closely related to the collection of discriminative muscular activities of numerous hand motions. But seldom studies focus on the improvement of the electrode configuration. It is reported that motion recognition rate is sensitive to the placement of sEMG electrodes and electrodes displacements degrade the sEMG signals.[11–13] This paper implements an electrode sleeve that optimizes the number of electrodes and its distribution on the forearm. Second, sEMG signal is susceptible to noises, interferences and artefacts, which result in the faulty identifying intended motions. This paper designs the hardware and firmware to prohibit the adverse effect on the stage of signal amplification. Finally, EMG feature extraction plays a crucial role in the success of hand motion recognition rather than classifiers.[14–16] The proposed feature differential root mean square (DRMS) that modified from root mean square (RMS) proves that slight change of EMG feature can greatly improve motion classification accuracy.

The remainder of the paper is structured as follows. Section 2 describes the setup of the multichannel sEMG electrode configuration and the supporting hardware and software. Section 3 presents the novel EMG presentation in a 2D EMG map which can be simultaneously generated in real-time. Section 4 demonstrates the success of the proposed system and features for hand motion recognition.

2. SEMG Signal Acquisition System Setup

2.1. *The configuration of 16-channel sEMG electrode array*

Detecting signals on the skin with a number of point-like electrodes means sampling the potential distribution,[17] and the recorded signal is sEMG signal. Monopolar montage and bipolar montage are two electrode configurations for sEMG signal acquisition. On the one hand, Staudenmann *et al.*[18] demonstrates that monopolar montage signals show a strongly homogeneous pattern over the muscle, while the bipolar montage shows a less homogeneous pattern. In other words, bipolar montage provides better discriminative sEMG signals than monopolar montage. On the one hand, bipolar montage has better performance than monopolar montage owning to the shorter distance between two electrodes. On the other hand, with the same number of single electrodes, monopolar montage can obtain more sEMG channels than bipolar, which reduces the complexity of electrodes layout. This paper employs a new electrode distribution that combines the advantage of the bipolar montage and the monopolar montage through sharing one electrode in adjacent EMG channel, as shown in Fig. 1. The total 16 channels are divided into two halves, named two rings. In one ring, the sEMG signals are gathered from neighboring two electrodes, and one electrode is shared by two EMG channels.

The electrodes in our system are modified from standard disposable Ag/AgCl ECG electrodes by means of gel removing. Electrodes are evenly fixed on an elastic fabric in advance. The procedure of arranging the electrodes on the forearm is as simple as wearing a sleeve. An empty sleeve (without electrodes on it) covers the

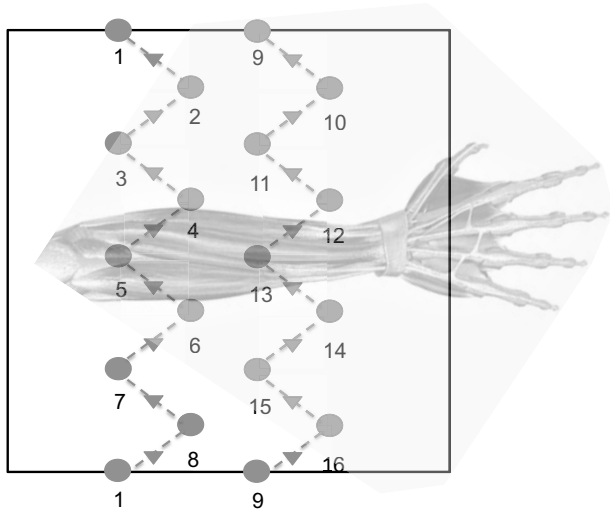

Fig. 1. (Color online) The distribution of electrodes on a 2D space. Blue solid circles labeled from 1 to 16 are the electrodes. A red triangle indicates a bipolar EMG channel that collects two neighboring electrodes by dot lines.

previous one to guarantee a proper electrode to skin impedance. Before wearing the electrodes sleeve, subjects are obliged to wash their forearm for better electrode to skin impedance as well.

2.2. *SEMG signal amplifier*

SEMG signal is easy to get contaminated by various noises, such as power line interference,[19] baseline wander and motion artefacts,[20] amplifier saturation, poor electrode contact, physiologic interference and so forth. Besides, sEMG signal is very weak comparing with these noises, e.g., the power line noise is approximately 1000 times stronger than the sEMG signal in office environments. Therefore, signal amplification circuit should be carefully designed for noise removing. A single channel sEMG signal circuit consists of a low-pass filter, an instrumentation amplifier, a band-pass filter, a notch filter, a main amplifier and a level uplifting circuit, shown in Fig. 2. The sEMG signal amplifier (shown in Fig. 2) only demonstrates one sEMG channel. For a 16-channel system, the equivalent circuit is copied 16 times mechanically to form a 16-channels sEMG acquisition system. Finally, an ADC is employed to convert analogy signal to a digital signal for further processing and analysis.

2.3. *Signal processing and display*

A microcontroller (STM32L151V8 by STMicroelectronics Inc.) is used to complete the tasks of converting signals from analogy to digital and packaging digital sEMG signals to a USB parcel. Figure 3 demonstrates the sEMG signal data stream in firmware and software.

In this paper, sEMG signal sampling frequency is set to 1 kHz, which is twice higher than the maximum frequency of sEMG signals and conforms to the Nyquist sampling theorem. The newly received data with 16 channels are put into a buffer

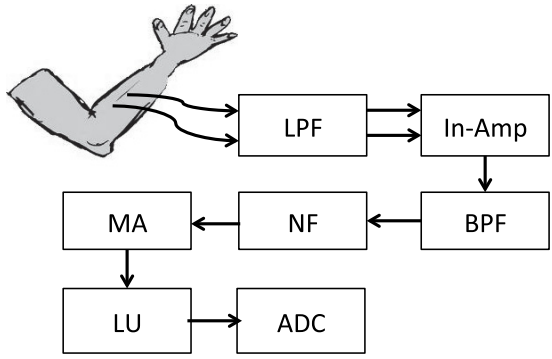

Fig. 2. The flowchart of an sEMG analogy circuit. LPF, BPF and NF indicate a low-pass filter, a band pass filter and a notch filter, respectively. In-Amp and MA mean an instrumentation amplifier and a main amplifier. LU denotes a level uplifting circuit.

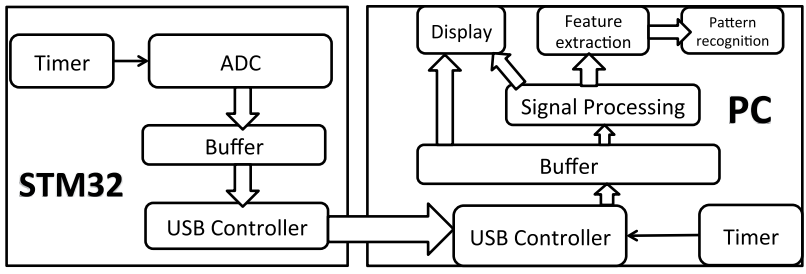

Fig. 3. Software and firmware structure that runs in a microcontroller and a PC.

under a customized format. Once the buffer is full, a data parcel would be copied to a special buffer in the USB unit and prepared to be read by the USB host in a PC (shown in Fig. 3). In order to guarantee real-time performance, the USB buffer is updated no matter the data are read or not. In the PC end, a customized USB driver is designed for USB communication between an EMG device and a PC. This USB driver serves the application software that undertakes the responsibilities of sEMG signal display, saving and processing. The software structure is depicted in Fig. 3.

3. Real-time 2D EMG Map Display

Traditionally, sEMG signals are displayed in curves that display signal amplitudes along with time axis, as such it is capable of showing the EMG signal in a temporal domain. However, it is limited to the demonstration of the spacial relationship between channels in a multichannel sEMG system. Therefore, this paper proposes a method to represent forearm multichannel sEMG signal in the form of 2D EMG maps, as seen in Figs. 4 and 5. In an EMG map, there are 16 annular sectors distributed in two annulars, inner-annular and extra-annular. On each annular, there

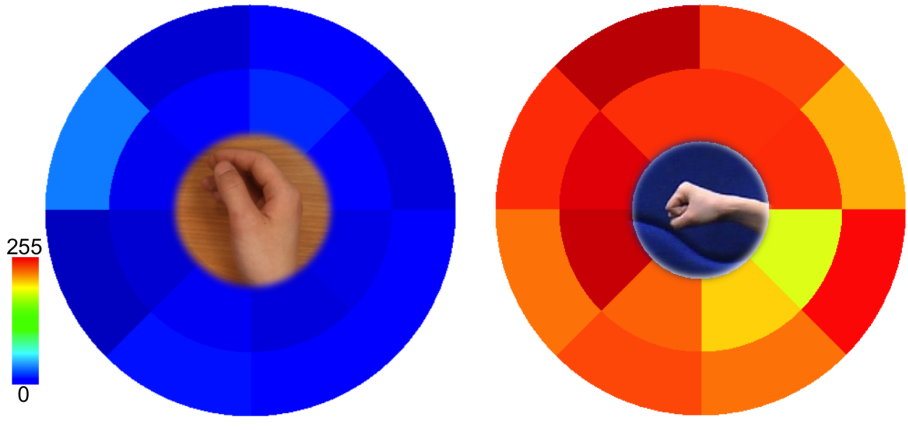

Fig. 4. It shows the EMG map under hand rest and hand close.

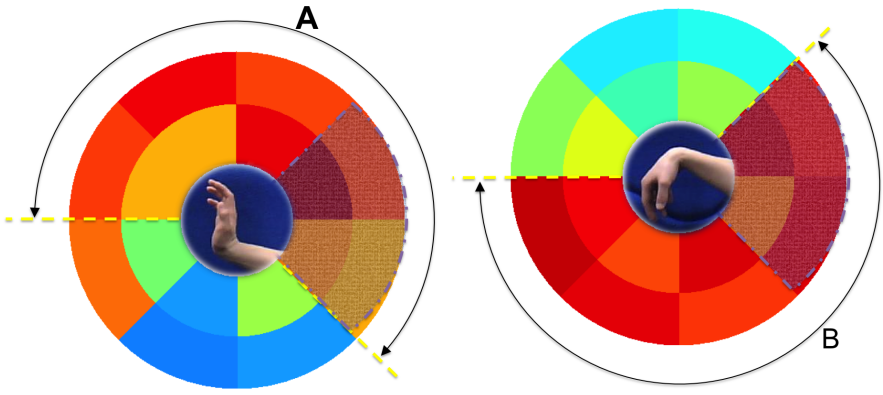

Fig. 5. It shows the sEMG map of two wrist motions. Range A shows the main muscle area that contributes to wrist extension, and B shows the main muscle area that contributes to flexion motion.

are eight annular sectors, and one annular sector represents one sEMG channel. The location of each annular sector is associated with electrode positions on the forearm. The extra-annular represents the proximal sEMG channels, ranging from channel 1 to 8, and the inner-annular represents the sEMG channels near to the hand, which ranges from channel 9 to 16 (seen in Fig. 1).

The color of each annular sector reflects sEMG signal intensity, which is weighed by normalized RMS values, calculated in Eqs. (1) and (2).

$$\mathrm{RMS}_{\mathrm{normalized}} = \frac{\ln(\mathrm{RMS}) - \ln(\mathrm{RMS}_{\min})}{\ln(\mathrm{RMS}_{\max}) - \ln(\mathrm{RMS}_{\min})} \times 255, \tag{1}$$

$$\mathrm{RMS}(j) = \sqrt{\frac{1}{N} \sum_{i=jL+1}^{N+jL} x_i^2}, \tag{2}$$

where x_i, N, L are the raw sEMG signal, segmentation window size and the length of interval, respectively. This paper applies a logarithmic scale to the RMS value, which is used to better separate transient and steady-state EMG signals. In addition, each sEMG channel is normalized to MAX on a scale of 0 to 255.

This paper sets the window size N to 300 ms and interval L to 20 ms, which has been widely accepted to guarantee systems' real-time performance.[21,22] The maximum and minimum value for each channel is updated while the received *RMS* beyonds current boundary values. Software runs in a PC installed Windows XP Service Pack 3 with 3 GHz Core 2 CPU and 3 GB memories. Two groups of hand motions are completed in the experiments. The first group is to check whether all channels can capture muscular activities by two hand motions: hand relax and hand close (shown in Fig. 4). The second group is to show the changes of graphic patterns with two wrist motions: wrist flexion and wrist extension (shown in Fig. 5).

In Fig. 5, it is easy to identify the borders that separate EMG map into two sections. One section contributes to flexion and the other contributes to extension. This

multichannel sEMG signal representation is more intuitive than the traditional one, and it benefits the observation of sEMG signals in real-time, especially for multichannel sEMG signals captured from evenly distributed electrode configuration.

4. Hand Motion Classification

4.1. *Data capturing and processing*

During data collection, one subject sits in a chair facing the experimental desk after wearing the sEMG electrode sleeve and a cyberGlove that measures the angles of every degree of freedom of the hand. The subject is asked to perform four hand motions using the thumb to touch other fingers, as shown in Fig. 6. The subject repeats each motion during a period of 60 s. It should be noted that there are no restrictions on the repeating times, exerting force and motion speed in our experiment, which contributes to a more general sample bank. Therefore, a classifier trained by this sample bank could be more robust.

The captured sEMG signal consists of four phases: The relax state of a hand, the dynamic procedure for forming a gesture, the steady state for maintaining a hand motion and the dynamic procedure for releasing a gesture.[23,24] This paper only utilizes the sEMG signal within a steady state to recognize hand motions. To extract the static state from a continuous sEMG signal, this paper takes advantage of the angle signal recorded by the CyberGlove system. First, the angle channel with the biggest variance is chosen to extract the static state sEMG signal. Secondly, calculate the sEMG signal gradient for the selected channel. Thirdly, apply a threshold filter to the gradient value to obtain clear spikes. The last step is to find the starting points and ending points for every trial according to the fact that a positive spike is

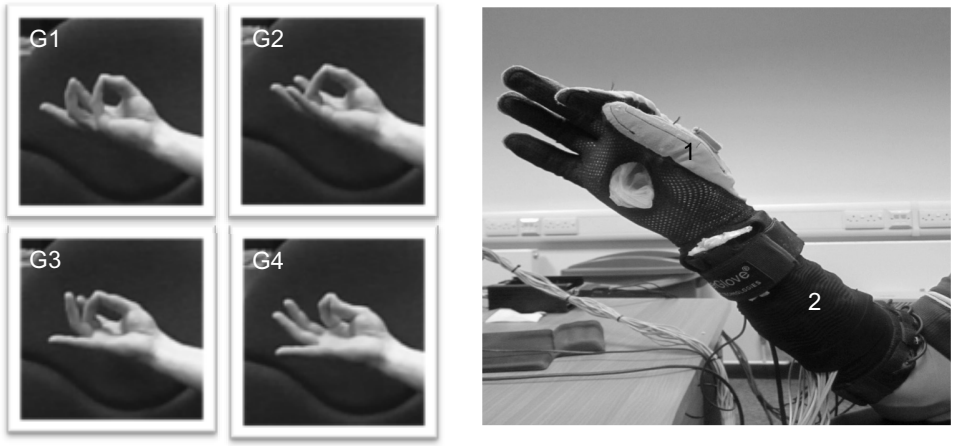

Fig. 6. The left part demonstrates the definition of four hand gestures, G1, G2, G3 and G4. The right part shows the experimental scene, where 1 and 2 indicates the Cyberglove and the sEMG system, respectively.

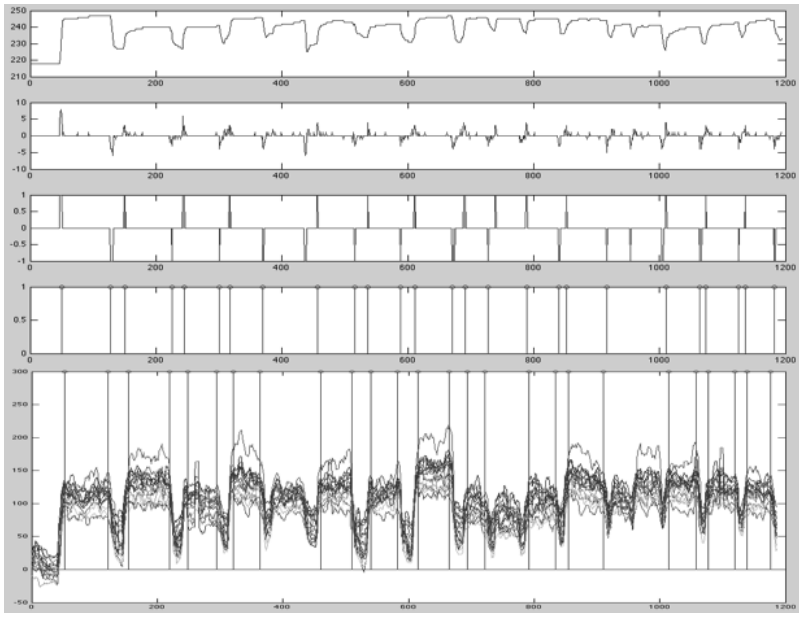

Fig. 7. This figure shows the evolution of attaining the starting and endin points from raw angle information. The first row is the raw angle signal with the maximum variance among all angle signal channels. The second row indicates the gradient of the above one. The third row shows the signal after applying a threshold filter. The fourth row shows successfully obtained boundaries after removing the unnecessary spikes. The last row shows the success in applying the narrowed boundaries to a sEMG signal.

likely to be followed by a negative spike. If there are several consecutive positive spikes, the last one would be chosen, and if there are several consecutive negative spikes, the first one would be chosen. In addition, to remove the instantaneous sEMG as much as possible, this paper moves every starting point 20 ms later and end point 20 ms ahead. A signal evolution from raw angle signal to the extracted starting and ending points is shown in Fig. 7.

4.2. *Compare RMS with DRMS*

RMS is a typical EMG amplitude estimator,[25] which is one of the most important time domain features for EMG signal analysis because of lower computational cost and decent performance. The reflected characteristics of sEMG signals by RMS are similar to other time domain features, like integral absolute value (IAV), mean absolute value (MAV) and so forth. It is reported that these time domain EMG features have equivalent performance in hand motion recognition.[15] Frequency domain features usually involve signal transformation, so it takes heavy computing burden. Furthermore, frequency domain features, such as Median frequency and

Mean frequency, do not show any advantage in Refs. 15 and 26. Therefore, this paper selects RMS as a representative to implement experiments. The calculation of RMS is given in Eqs. (1) and (2), which includes nonlinear scale transformation and signal normalization.

However, RMS only gauges the characteristic of a single EMG signal. Literatures have started to take the relationship between different EMG channels into account as multichannel EMG systems become popular.[16] Inspired from the EMG 2D map, this paper presents a new EMG feature DRMS that measures the difference of two neighboring EMG signals. It is closely consistent with the characteristics of human vision system that human eyes concentrate more on the changing parts of a image or a video rather than the static signals. DRMS just extracts the changing parts of a 2D EMG map in a spacial domain and it is closely related to the distribution of sEMG electrodes on the forearm. The calculation of **DRMS** feature vector is given in Eqs. (3)–(6) as below.

$$\mathbf{RMS} = [\mathrm{RMS}_1, \mathrm{RMS}_2, \ldots, \mathrm{RMS}_{16}], \tag{3}$$

$$\mathbf{DRMS} = [\mathbf{DRMS}_1, \mathbf{DRMS}_2], \tag{4}$$

$$\mathbf{DRMS}_1 = [\mathrm{RMS}_1 - \mathrm{RMS}_2, \mathrm{RMS}_2 - \mathrm{RMS}_3, \ldots, \mathrm{RMS}_8 - \mathrm{RMS}_1], \tag{5}$$

and

$$\mathbf{DRMS}_2 = [\mathrm{RMS}_9 - \mathrm{RMS}_{10}, \mathrm{RMS}_{10} - \mathrm{RMS}_{11}, \ldots, \mathrm{RMS}_{16} - \mathrm{RMS}_9], \tag{6}$$

where **RMS** stands for a row vector with 16 scale values RMS_1–RMS_{16}. **DRMS** consists of two row vectors, $\mathbf{DRMS}_1$ and $\mathbf{DRMS}_2$ containing 8 scale values.

Figure 8 demonstrates the samples in a 2D spaces, of which the sample dimension is reduced to two by principle component analysis. By contrast of Figs. 8(a) and 8(b), it is clear that DRMS has better discrimination between four hand motions than that

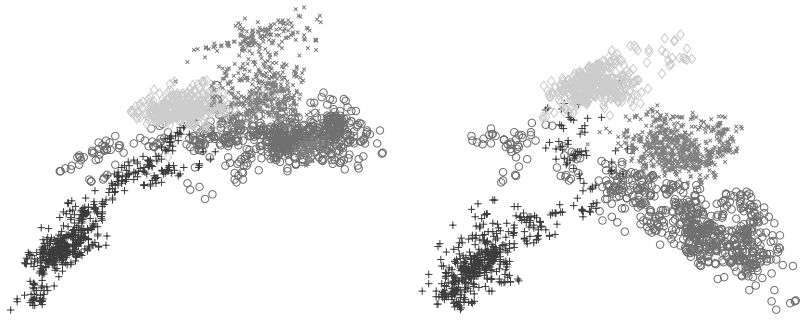

(a) (b)

Fig. 8. (Color online) It contrasts on the features RMG (a) and DRMS (b) in a 2D spaces. 2089 samples (G1 637, G2 484, G3 372 and G4 596) are employed to draw the scatter figure. Red ∘, blue +, green and magenta × stand for hand motion G1, G2, G3 and G4, respectively. To demonstrate a 16D feature vector in 2D space, principal component analysis is used to reduce the feature dimension to 2. (a) RMS, (b) DRMS.

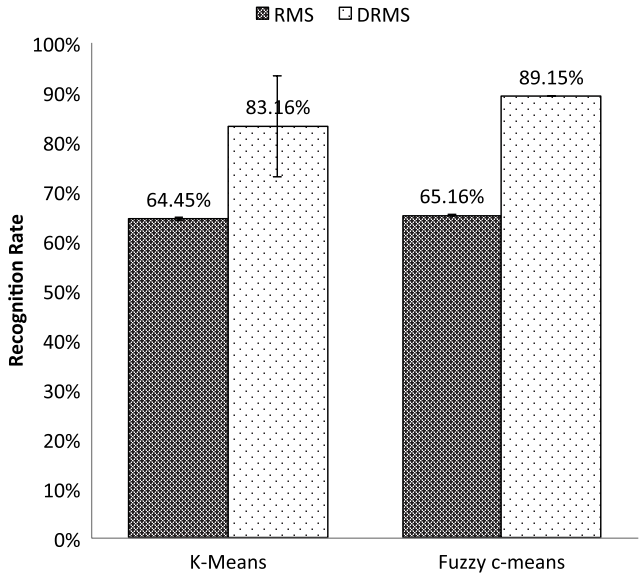

Fig. 9. A comparison result with the features of RMS and DRMS in K-means and fuzzy C-means clustering algorithm for four hand gestures.

of RMS. Furthermore, two clustering algorithms (K-means and fuzzy C-means) are selected to validate the advantages of DRMS. To implement the algorithms, all the samples are mixed together, and K-means and fuzzy C-means are employed to separate these samples into four clusters. The numbers of sample points of four hand motions in each cluster are counted, and the motion with the biggest number in a cluster is considered as the class of the corresponding cluster. The hand motion classification accuracy of 10 runs of both algorithms fed by RMS and DRMS are depicted in Fig. 9. It is notable that feature DRMS outperforms RMS by 29.0% and 36.8% in K-means and fuzzy C-means clustering, respectively.

5. Discussion and Conclusion

This paper proposes a 16-channel sEMG capturing system for hand motion recognition, and the framework of the hardware and software is introduced. The proposed electrode configuration is similar to sEMG sensor ring/band, which ignores the process of muscles positioning.[8,27,28] Different from these designs, it covers most of the muscles on the forearm with limited number of electrodes. It is widely accepted that increasing the EMG channel number can increase the accuracy of hand motion classification, but whether the cost of more electrodes and heavier computing burden worth the limited improvement is still unsure.[29–31] 16 electrodes and 16 EMG channels perhaps a tradeoff between the hardware cost and system performance.

This paper also presents an EMG map to demonstrate the forearm muscle activities in a temporal-spacial space according to the specific characteristics of the

sEMG electrodes. Experiments have been undertaken to show the potential of the EMG map. The steady EMG maps of hand rest, hand close, wrist extension and wrist flexion are discriminative. Through observation of the changing EMG map with different hand motions, the differences between neighboring EMG channel on the EMG map are more obvious than that of the colors in separate EMG channels. Inspired by this, the feature DRMS is discovered, which considers the relationship between neighboring sEMG channels. However, all the features compared in Ref. 15 do not take account of the relationship between each channel. Although some may argue that advanced classifiers have already utilized these relationships automatically, utilizing these relationships in advance can certainly narrow the computational cost and the demand of pattern recognition methods. The comparison results show that DRMS outperforms RMS in the task of four hand motion sEMG data clustering. This result is consistent with studies in Refs. 16 and 32, both of which prove that the relationships or correlations between different EMG channels provide a vast amount of external hand motion related information. Generally, DRMS is a special case of the gradient of the EMG map in a space domain. The achieved results suggest that robust and discriminative EMG features can be extracted in the light of this approach. The exploration of the relationships between separate channels will contribute to the accuracy and stability of EMG based hand motion recognition.

Further research will employ more subjects and conduct more hand motions for data collection and validation. In this paper, the participants hold their hands in a steady state to provide instances, but people may perform hand gestures with different arm positions in practice. Therefore, further methodology will take the factor of arm position into account. Regardless of the fact that the EMG map can be displayed on the screen in real-time, the analysis of EMG-based hand motion recognition is still off-line. Thus, more efforts should be done to establish a real-time framework that integrates the current system with machine learning methods.

Acknowledgments

This research was supported by grants of the UK Engineering and Physical Science Research Council (Grant No. EP/G041377/1), the National Basic Research Program (973 Program) of China (Grant No. 2011CB013305) and the Science and Technology Commission of Shanghai Municipality (Grant No. 13430721600).

References

1. N. Jiang, D. Falla, A. d'Avella, B. Graimann and D. Farina, Myoelectric control in neurorehabilitation, *Crit. Rev. Biomed. Eng.* **38**(4) (2010) 381–91.
2. X. Zhang, X. Chen, Y. Li, V. Lantz, K. Q. Wang and J. H. Yang, A framework for hand gesture recognition based on accelerometer and emg sensors, *IEEE Trans. Syst. Man Cybernet. Part A — Syst. Humans* **41**(6) (2011) 1064–1076.
3. Z. J. Ju, X. Y. Zhu and H. H. Liu, Empirical copula-based templates to recognize surface emg signals of hand motions, *Int. J. Humanoid Robot.* **8**(4) (2011) 725–741.

4. M. H. M. Zaini and S. A. Ahmad, Surgical and non-surgical prosthetic hands control: A review, 25–28 September 2011, pp. 634–637.
5. L. Hargrove, K. Englehart and B. Hudgins, A training strategy to reduce classification degradation due to electrode displacements in pattern recognition based myoelectric control, *Biomed. Signal Process. Control* **3**(2) (2008) 175–180.
6. Z. J. Ju and H. H. Liu, A unified fuzzy framework for human-hand motion recognition, *IEEE Trans. Fuzzy Syst.* **19**(5) 901–913, 2011.
7. Z. Ju and H. Liu, Recognizing hand grasp and manipulation through empirical copula, *Int. J. Social Robot.* **2**(3) 321–328, 2010.
8. Y.-C. Du, C.-H. Lin, L.-Y. Shyu and T. Chen, Portable hand motion classifier for multi-channel surface electromyography recognition using grey relational analysis, *Expert Syst. Appl.* **37**(6) (2010) 4283–4291.
9. G. R. Naik, D. K. Kumar, S. P. Arjunan and M. Palaniswami, Independent component approach to the analysis of hand gesture semg and facial semg, *Biomed. Eng.-Appl. Basis Commun.* **20**(2) (2008) 83–93.
10. X. Chen, X. Zhang, Z.-Y. Zhao, J.-H. Yang, V. Lantz and K.-Q. Wang, Multiple hand gesture recognition based on surface emg signal, in *The 1st Int. Conf. Bioinformatics and Biomedical Engineering, 2007. ICBBE 2007*, IEEE, Conference Proceedings (2007), pp. 506–509.
11. L. Hargrove, K. Englehart and B. Hudgins, A training strategy to reduce classification degradation due to electrode displacements in pattern recognition based myoelectric control, *Biomed. Signal Process. Control* **3**(2) (2008) 175–180.
12. L. Hargrove, K. Englehart and B. Hudgins, The effect of electrode displacements on pattern recognition based myoelectric control, *Conf. Proc. IEEE Eng. Med. Biol. Soc.* **1** (2006) 2203–6.
13. B. Hudgins, P. Parker and R. N. Scott, A new strategy for multifunction myoelectric control, *IEEE Trans. Biomed. Eng.* **40**(1) (1993) 82–94.
14. E. C. Orosco, N. M. Lopez and F. di Sciascio, Bispectrum-based features classification for myoelectric control, *Biomed. Signal Process. Control* **8**(2) (2013) 153–168.
15. A. Phinyomark, F. Quaine, S. Charbonnier, C. Serviere, F. Tarpin-Bernard and Y. Laurillau, Emg feature evaluation for improving myoelectric pattern recognition robustness, *Expert Syst. Appl.* **40**(12) (2013) 4832–4840.
16. X. Tang, Y. Liu, C. Lv and D. Sun, Hand motion classification using a multi-channel surface electromyography sensor, *Sensors (Basel)* **12**(2) (2012) 1130–47.
17. R. Merletti, M. Aventaggiato, A. Botter, A. Holobar, H. Marateb and T. M. Vieira, Advances in surface emg: Recent progress in detection and processing techniques, *Crit. Rev. Biomed. Eng.* **38**(4) (2010) 305–45.
18. D. Staudenmann, I. Kingma, D. F. Stegeman and J. H. van Dieen, Towards optimal multi-channel emg electrode configurations in muscle force estimation: A high density emg study, *J. Electromyogr. Kinesiol* **15**(1) (2005) 1–11.
19. M. Malboubi, F. Razzazi and S. M. Aliyari, Elimination of power line noise from emg signals using an efficient adaptive laguerre filter, in *2010 Int. Conf. Signals and Electronic Systems (ICSES)*, Conference Proceedings, 2010, pp. 49–52.
20. C. J. De Luca, L. D. Gilmore, M. Kuznetsov and S. H. Roy, Filtering the surface emg signal: Movement artifact and baseline noise contamination, *J. Biomech.* **43**(8) (2010) 1573–1579.
21. K. Momen, S. Krishnan and T. Chau, Real-time classification of forearm electromyographic signals corresponding to user-selected intentional movements for multifunction prosthesis control, *IEEE Trans. Neural Syst. Rehabil. Eng.* **15**(4) (2007) 535–542.

22. K. Englehart and B. Hudgins, A robust, real-time control scheme for multifunction myoelectric control, *IEEE Trans. Biomed. Eng.* **50**(7) (2003) 848–854.
23. D. P. Yang, J. G. Zhao, L. Jiang and H. Liu, Dynamic hand motion recognition based on transient and steady-state EMG signals, *Int. J. Humanoid Robot.* **9**(1) (2012) 1250007.
24. S. K. Chen, M. T. Wu, C. H. Huang, J. H. Wu, L. Y. Guo and W. L. Wu, The analysis of upper limb movement and EMG activation during the snatch under various loading conditions, *J. Mech. Medi. Biol.* **13**(1) (2013) 1350010.
25. A. Phinyomark, F. Quaine, Y. Laurillau, S. Thongpanja, C. Limsakul and P. Phukpattaranont, EMG amplitude estimators based on probability distribution for muscle-computer interface, *Fluctuation Noise Lett.* **12**(3) (2013) 1340016–8.
26. R. Boostani and M. H. Moradi, Evaluation of the forearm emg signal features for the control of a prosthetic hand, *Physiol. Meas.* **24**(2) (2003) 309–319.
27. T. S. Saponas, D. S. Tan, D. Morris and R. Balakrishnan, Demonstrating the feasibility of using forearm electromyography for muscle-computer interfaces, in *Chi 2008: 26th Annual Chi Conference on Human Factors in Computing Systems*, Vols. 1 and 2, Conference Proceedings (2008) 515–524.
28. M. Rojas-Martinez, M. A. Mananas and J. F. Alonso, High-density surface EMG maps from upper-arm and forearm muscles, *J Neuroeng. Rehabil.* **9** (2012) 85.
29. R. N. Khushaba, A. Al-Ani and A. Al-Jumaily, Orthogonal fuzzy neighborhood discriminant analysis for multifunction myoelectric hand control, *IEEE Trans. Biomed. Eng.* **57**(6) (2010) 1410–9.
30. H. Daley, K. Englehart, L. Hargrove and U. Kuruganti, High density electromyography data of normally limbed and transradial amputee subjects for multifunction prosthetic control, *J. Electromyogr. Kinesiol* **22**(3) (2012) 478–84.
31. S. Muceli and D. Farina, Simultaneous and proportional estimation of hand kinematics from emg during mirrored movements at multiple degrees-of-freedom, *IEEE Trans. Neural Syst. Rehabil. Eng.* **20**(3) (2012) 371–8.
32. G. X. Ouyang, Z. J. Ju and H. H. Liu, Changes in EMG-EMG coherence during hand grasp movements, *Int. J. Humanoid Robot.* **11**(1) (2014) 1450002.